NANO LETTERS

2007
Vol. 7, No. 7
2146−2151

Direct Force Measurements and Kinking under Elastic Deformation of Individual Multiwalled Boron Nitride Nanotubes

Dmitri Golberg,*,† Pedro M. F. J. Costa,† Oleg Lourie,§ Masanori Mitome,† Xuedong Bai,‡,|| Keiji Kurashima,† Chunyi Zhi,‡ Chengchun Tang,† and Yoshio Bando†,‡

Nanoscale Materials Center, International Center for Young Scientists, National Institute for Materials Science, Namiki 1-1, Tsukuba, Ibaraki 3050044, Japan, and Nanofactory Instruments AB, Walleriusgatan 2, SE-41285 Göteborg, Sweden

Received April 12, 2007; Revised Manuscript Received May 14, 2007

ABSTRACT

Individual multiwalled boron nitride nanotubes of different diameters (40–100 nm) were bent inside a 300 kV high-resolution transmission electron microscope (TEM) using a new fully integrated TEM–atomic force microscope (AFM) piezodriven holder under continuous recording of force–piezodisplacement curves. The tubes were gently compressed in situ (i.e., inside the electron microscope) between a piezomovable aluminum wire and a silicon cantilever. Typically, bending stress values ranging from ∼100 to ∼260 MPa, and corresponding to elastic moduli of 0.5–0.6 TPa, were estimated. Tube gross failures were absent up to very large bending angles (in excess of 115°). Extending the bending angles beyond 30–40° resulted in the elastic deformation of BN nanotubes, which proceeded through the propagation of consecutive momentary kinks. These had the effect of accumulating a bending curvature rather then uniformly curl the tube under the compression load. These kinks were found to be entirely reversible on reloading with no (or marginal) traces of residual plastic deformation.

A boron nitride nanotube (BNNT) is a structural analog of a carbon nanotube (CNT) in which alternating B and N atoms entirely substitute for C atoms in a honeycomb lattice.[1] BNNTs are an intriguing nanoscale material. For instance, in spite of the fact that BNNT is an electrical insulator with a 5.5 eV band gap,[2] its electrical response can be tuned by doping or deformation.[3,4] BNNTs have also shown piezoelectric behavior.[4,5] In addition, BNNTs may find interesting uses in polymeric composites,[6] with potential to rival or even surpass CNTs due to their superior thermal and chemical stabilities, straight shapes, superb rigidity, and elasticity. Thus understanding the mechanical response of BNNTs is a very important "nano"-related technological issue. However, to date, the mechanical behavior of BNNTs has remained basically unexplored. It is worth noting that, for multiwalled and singlewalled CNTs, several quantitative experimental tests on bending, compressive, or tensile deformations have been performed[7−18] and compared with theoretical estimates and computations.[19−21] For example, a scanning electron microscope (SEM) equipped with deformation and manipulation stages,[11−13] scanning tunneling microscope (STM)−TEM,[15−17] and atomic force microscopes (AFM)[7,10] setups have been employed to measure plastic and elastic deformation parameters of CNTs. By contrast, for the particular case of BNNTs, theoretical studies have been far ahead of experimental ones. It is worth noting that the computations have yielded a number of interesting results.[22−24] Accordingly, the Yakobson's group at Rice University theoretically treated a plastic yield of individual single BN tubular shells and found that the 5/7/7/5 dipoles (the movement of which governs the nanotube deformation/shape variations) appeared to be energetically more favorable compared to the 4/8/8/4 counterpart. This is surprising because the latter configuration would proceed through the generation of homoelemental B−B and N−N bonds, which are known to be less stable than the B−N ones and therefore intuitively expected to be thermodynamically unfavored.[22] Compared to CNTs, the formation energy of such primary defects was found to be higher and furthermore remained positive for large strains, thus suggesting the greater yield stress of BNNTs. Oppositely, the activation energy of such defects was calculated to be lower in BNNTs, implying a more thermomechanically stable behavior at elevated temperatures (or long deformation times).[23,24] Also noteworthy, in terms of the elastic behavior for small single-layered tubes of matching radius, the strain energy for CNTs was computed to be larger than that for

* Corresponding author. E-mail: golberg.dmitri@nims.go.jp.
† Nanoscale Materials Center.
‡ International Center for Young Scientists.
§ Nanofactory Instruments AB.
|| Present address: Institute of Physics, Chinese Academy of Sciences, Beijing 100080, China.

10.1021/nl070863r CCC: $37.00
Published on Web 06/01/2007

BNNTs, while for large tubes, the opposite was assumed to be true.[21] In fact, the strain energy for BNNTs was calculated to become larger than that for CNT at $n > 40$ for (n,n), i.e., armchair, type tubes.

With respect to the experimental verification of mechanical differences versus similarities of BNNTs and CNTs, there have been very few experiments. In one such study, Chopra and Zettl[25] first measured the elastic modulus of multiwalled BNNTs using an alternating current (ac) mechanical resonance technique inside a TEM and obtained values comparable to those of multiwalled CNTs. Additionally, we have recently evaluated the superb multiwalled BNNT flexibility under in situ experiments with a STM−TEM Nanofactory Instruments probing system.[26] However, the latter system, while readily providing the opportunity for precise and well-controlled tube bending/manipulation in tandem with $I-V$ curve recording under the high-resolution visual monitoring of nanostructure changes, does not allow the extraction of the numerical parameters of deformation. A novel integrated AFM−TEM holder equipped with a MEMS force sensor has finally enabled the in situ and straightforward quantitative measurements of the mechanical characteristics of various nanostructured materials.

Thus, in the present work and for the first time, we performed the direct force measurements under bending of highly pure, well-structured multiwalled BNNTs of various diameters inside a 300 kV high-resolution field-emission JEOL transmission electron microscope. This allowed us to unambiguously evaluate the bending stresses and to estimate the elastic modulus of individual BNNTs while carefully surveying for possible tube lattice changes during elastic bending. In addition, the real-time video recording of the in situ deformation process allowed us to follow uninterruptedly the sequence and time scale of the BNNT buckling/kinking phenomena that took place due to the applied large bending forces.

Multiwalled BNNTs were fabricated in line with an induction-heating procedure that has been successfully utilized in our laboratory in recent years.[26,27] The force measurement experiments were carried out using a new state-of-the-art atomic force microscope (AFM)−transmission electron microscope (TEM) holder commercialized by Nanofactory Instruments AB.[28] The holder was arranged within a 300 kV high-resolution field-emission TEM JEM-3000F. An experimental setup is sketched in Figure 1. A silicon cantilever was attached to a fixed MEMS force sensor, whereas an aluminum wire with a mounted BNNT sample was placed on the piezomovable side of the holder. Initially, the wire and cantilever relative positions were manually adjusted with tweezers under an optical microscope in order to obtain the minimal possible gap distinguished by eye between them. Finally, the X, Y, and Z positions of the cantilever and each individual BN nanotube of interest were adjusted through the nanoscale precision piezodriven manipulation of the sample wire inside TEM. The motion of the sample and force-acquisition parameters were programmed and controlled by the dedicated software and electronics from Nanofactory Instruments AB. This PC-compatible software automatically coordinates the final stages, leading to control of the BNNT sample displacement in addition to controlling the deformation rate. Before the key data measurements of BNNT bending forces, the load−piezodisplacement curves were recorded and calibrated by means of the indentation of a blank Al wire, and relevant coefficients were introduced into the software menu. All bending processes were videorecorded in real-time using a TV-rate charge-coupled device (CCD) camera with a 30 frames/s recording speed. During the experiments, we have carefully monitored the development of the force-deformation process in individual BNNTs up to the bifurcation points during compressive bending/buckling. On the basis of the model adopted from the classical mechanics,[14,17,18,29,30] the elastic modulus of BNNTs undergoing deformation has been evaluated.

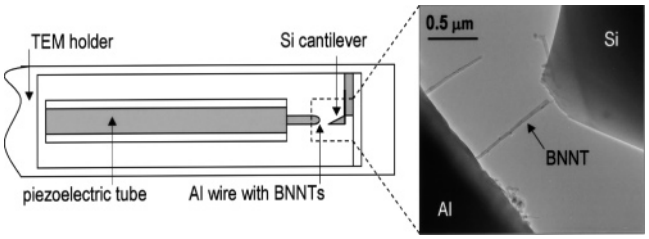

Figure 1. Schematics of the experimental setup within an AFM−TEM holder; the inset on the right shows a TEM view of the framed area where an individual multiwalled BN nanotube stretches between a sample wire and a silicon cantilever. The position of the tube against the cantilever may be precisely adjusted through piezodriven displacements of the sample wire.

Initially, we should note that the pure BNNTs used in the present work had some important structural differences as compared to the standard cylinder-like nanotube shapes (such as for regular well-graphitized CNTs). This should be taken into account while treating the deformation data. The complete structural and chemical characterization of the present BNNTs is provided in the Supporting Information and Figures S1 and S2. The existence of alternating black contrast wall domains (Figure S1a) reflects some pre-existing strain−stress fields within the pure BNNTs (Figure S1c), which is assumed to be due to the frequent coexistence of cylinder- and polygon-like BNNT cross-sectional domains.[31,32] The presence of faceted shells whose orientation may be different with respect to the incident electron beam of the TEM was clearly confirmed on numerous electron diffraction patterns taken, Figure S1b. In addition, faceted- and/or round-like cross-sectional domains were verified on a specially prepared cross-sectional BNNT sample for TEM imaging in which the tube circumference may be viewed edge-on rather than in-plane, Figure S2.

Figure 2 displays TEM images of two representative BNNTs used for in situ TEM deformations, which we have named herein "thick" and "thin". The thick tube has an external nominal diameter of 100 nm and a very narrow internal channel (of several nanometers only). The thin one has the external and internal nominal diameters of 40 and 12 nm, respectively. The typical lengths of tubes squeezed between the approaching Al lead and the Si cantilever were

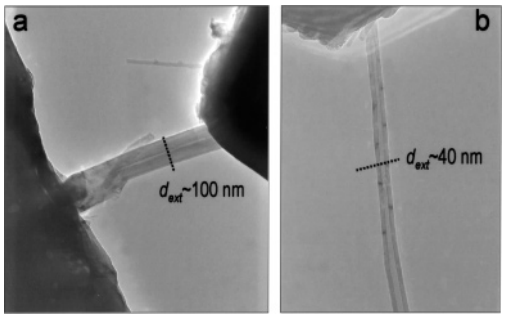

Figure 2. (a,b) TEM images of representative "thick" and "thin" individual multiwalled BN nanotubes that were mechanically probed in the course of the present work. The external nominal nanotube diameters are ~100 and ~40 nm, respectively, as marked in (a) and (b).

1−1.5 μm. It is noted here that, although numerous tubes have been measured, however, rarely were the experiments successfully accomplished due to hardly avoidable sliding of a BNNT over either Al or Si contact. That was accompanied with a notable loading force decrease. It makes the reliable statistical analysis of the data (including error analysis) rather difficult at this stage. Such sliding can only be prevented in the case of very tight physical contact between a tube and Al and Si mechanical clamps. The latter is favored when a given tube is oriented strictly perpendicular to the contact planes. However, that was not the dominant case and could not be precisely controlled during BNNT sample mounting and its further manipulations inside TEM. Actually, we should admit that the above-mentioned issue is a disadvantage of the present AFM−TEM technique as opposed to standard AFM. However, we found it useful to irradiate BNNT−Al and BNNT−Si interfacial areas with a convergent energetic TEM beam before mechanical testing. It has promoted a sort of "nanowelding" and on multiple occasions allows us to make reproducible tests, as documented below.

The original real force−piezo-BNNT-displacement curves during the deformation (taken at loading) of the thick and thin tubes are illustrated in Figure 3. The inset images are guides for the eye demonstrating the bending process during the Al wire approach to the Si cantilever. The applied deformation forces were directly measured to be ~900 and ~300 nN for the thick and thin tube, respectively. Keeping in mind the precise BNNT dimensions (i.e., internal and external "nominal" diameters and length, all accurately verified by HRTEM), it enabled us to estimate bending stresses of ~100 and ~260 MPa, respectively (herein we used the term "nominal" diameter because the exact cross-section of a tube under study is unknown and only its two-dimensional projection can be viewed during TEM). Moreover, the elastic modulus of the present tubes (in the range of small bending deformations) can also be evaluated using the Euler formula:

$$F_{\text{Euler}} = \pi^2 EI/L^2 \qquad (1)$$

where E is the Young modulus, I is the moment of inertia taken here as $I = \pi(d_2^4 - d_1^4)/64$ (where d_2 and d_1 are the external and internal nominal BNNT diameters, respectively), and L is the length of a BNNT between the two contacts. The calculated values were in the range of 0.5−0.6 TPa. These figures are indeed consistent with those previously determined by Suryavanshi et al. (0.722 TPa)[33] and by us (0.51 TPa)[34] using the well-established ac mechanical resonance technique[9,25] (see Supporting Information and Figure S3).

It is worth noting that the noise of the present AFM−TEM system (30−40 nN) is intrinsically higher than a standard optical AFM system operating on the bench.[7,10] This noise level depends on the electron doze and on the material of a nanotube supporting substrate because of the backscattered electrons. In contrast to conventional on-bench AFM, the present setup operates under a 300 kV electron beam and has a piezolever design that has fundamental noise limit around 1 nN due to intrinsic electronic noise in the resistors. Of course, the standard AFM optical detection is more sensitive, but it is not practical to fit it in 1.9 mm space between objective lenses of HRTEM.

Figure 4 consists of a series of selected frames extracted from the real-time video recordings made, where part of a cycle of the BNNT bending deformation process is displayed. As the gap between the approaching leads diminishes, the tube undergoes structural changes via the generation of consecutive sharp kinks rather than by uniform arclike tube bending as a whole. Once the kinks appear, further deformation is propagated by increasing the kink angle, which may reach ~90° (in the image plane) or even more, Figure 4e. Hereafter, we define a bending angle as the smaller angle between the tangents at the two ends of a kink. The kinks 1, 2, and 3 appear momentary within a millisecond time frame. They also quickly disappear in a springlike fashion and in exactly inverse sequence of reloading, leaving the tube after the load relief with an identical shape to the initial one, Figure 4a,h. Overall, this represents an unprecedented view of the multiple and fully reversible high-degree lattice deformation of BNNTs, whose internal structure is composed of randomly distributed heterogeneous geometry layers (tubular versus polygonal).

Importantly, the bending experiments inside TEM ultimately allow us to thoroughly trace the tubular lattice structural changes with an extremely high spatial resolution (up to ~1.7 Å) within an individual bent BNNT. This is an appealing advantage of the present novel in situ TEM techniques over the pre-existing AFM-[7,10] and SEM-based setups,[11−13,35] which have suffered from insufficient spatial resolution and thus left many deformation-related questions and mechanisms behind the elastic and/or plastic deformation unsolved. Each multiwalled BNNT kink was found to have a very complex structure of nonuniformly curved and highly corrugated graphitic-like BN layers. The initial perfect layer stacking (see Supporting Information and Figure S1d) had been severely distorted, as shown on a representative BNNT kink HRTEM image in Figure 5.

With respect to the limits of BNNT deformation, Figure 6 displays that a kink angle upon bending may reach more

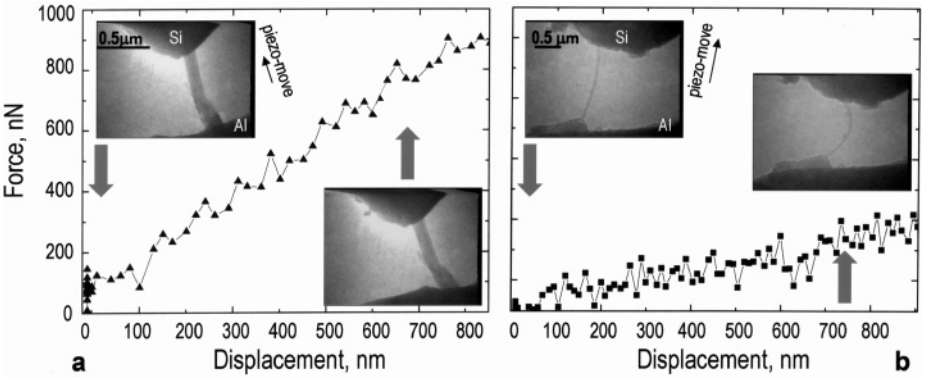

Figure 3. Force vs sample wire (i.e., nanotube) displacement curves recorded for the thick (a) and thin (b) BN nanotubes. The left and right insets on each curve display the appearance of the starting and bent nanotube morphologies. The intentional directions of piezodriven moves of an Al wire with the attached nanotube during the deformation are pointed out.

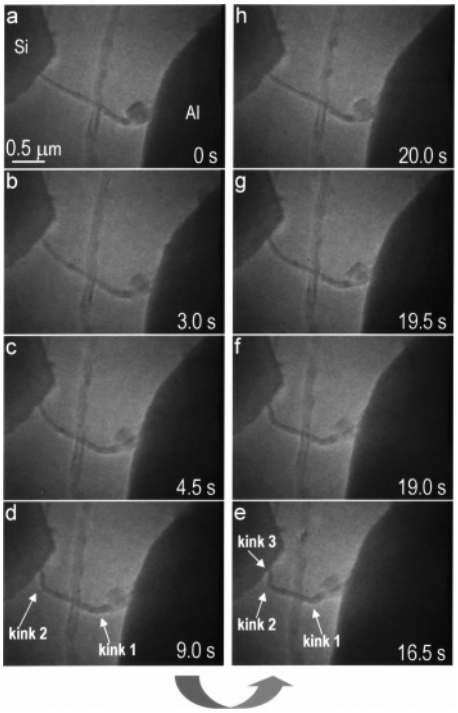

Figure 4. Sequence of real-time video frames (a−h) taken during approaching two sides of the setup and subsequent BN nanotube bending between them. With an increase in a bending curvature, the consecutive momentary kinks 1, 2, and 3 (d, e) appear on the tube, which entirely accommodate a bending deformation. The kinks momentary disappear (within dozens of milliseconds time) on reloading in a strictly reverse sequence as they appear on loading. Note that a crossing nanotube (in the center of view) is not in contact with the leads and does not take part in the present deformation process. The real time is marked on the frames.

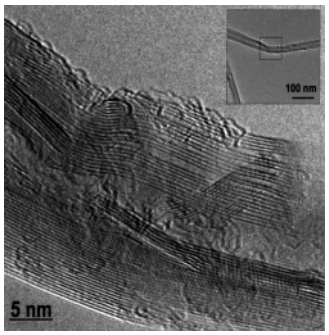

Figure 5. HRTEM image of a kinked BNNT displaying severe lattice-resolved structural deviations from a perfect layer-by-layer stacking characteristic of a starting BNNT (see Supporting Information and Figure S1d for comparison). Dislocation-like defects and numerous missing atomic planes within a highly deformed buckled BN walls are evident. The inset shows a low-magnification image of a kink where the area of interest is framed. The deformation kink structure itself becomes extremely complex provided by the above-mentioned variations in cross-section and helix type of multiple BN shells.

than 115° (on the image plane) without gross tube failure. The elastic forces may lead to a drastic tube position recovery in a springlike fashion within only ∼30 ms. However, after such a severe deformation, a sort of a residual plastic buckle, Figure 6c, is visible on a remaining freestanding tube, Figure 6d. This deformation is illustrated by a persistent ∼30° angle on the protruding BNNT. We note that, in many respects, the present BNNT deformation resembles that of CNTs, which has theoretically and experimentally been treated by several groups over the past decade.[7−18] For instance, molecular dynamics simulations compared with conventional TEM observations (of the tubes that were *unintentionally* bent during the sample preparation) have revealed that, during CNT bending, the tube straight shape may be fully reversible up to bending angles in excess of 110°, despite the formation of complex kink structures.[14] The first kinks were calculated to appear during CNT bending at angles around 30° and only beyond a bending angle of 120° bond-breaking mechanism starts to be in effect. Apart from such similarities, it is worth noting that, in a bent BN tube, e.g., Figure 4, the first kinks did not appear in the middle tube zone, where the maximum stresses−strains are presumed to take place. This unusual feature may reflect the above-mentioned peculiarities of a multiwalled BNNT cross-sectional shape, where the shells of various helixes and cross-sections may coexist, leading to the a priori strained regions, even on a nondeformed tube. In fact, such alternating areas with a characteristic stress−strain contrast (black contrast wall segments) are clearly seen in Figures 2b and S1a.

Buckling in bent cylindrical shells is a well-known phenomenon in continuum mechanics.[20,29] A single-kink collapse of a cylinder shell occurs as the bending moment

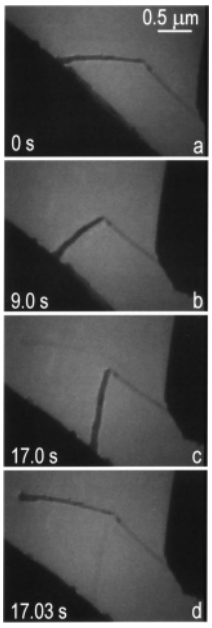

Figure 6. The consecutive real-time video frames of an individual BN nanotube high-angle bending (to the angles exceeding 115°), followed by a sudden and momentary (within 30 ms) springlike shape recovery, leaving a ~30° kink as residual plastic deformation.

reaches its maximum critical value and the shell becomes unstable, buckling sideways, while the force almost does not vary.[20] The present BNNT deformation picture seems to be much more complicated derived from the generally noncylinder but rather faceted BNNT shells, which additionally may possess various helicities (see Supporting Information and Figure S2b). Needless to say, atomistic modeling of multilayer, multihelix, multi-cross-section BNNT tube bending/buckling remains a very difficult and expensive challenge being presently a subject of our ongoing research.

In addition, we cannot fully rule out the effects of high-energy (300 kV) electrons on the peculiarities of BNNT defect formation versus their annealing-out and kinking, although it is difficult to evaluate such impact quantitatively at the present stage of experiments. In fact, it was demonstrated that intense electron irradiation may dramatically affect the mechanical response of single-walled carbon nanotube bundles[36] or initiate the dislocation glide in multiwalled BNNTs.[37] However, it is noted that the present multiwalled BNNTs were found to be much more robust to electron irradiation than CNTs (under electron current densities of ~1−2 A/cm^2 found under normal imaging conditions of the JEOL-3000F microscope), and we did not observe significant tube modifications, structural deterioration, amorphization, and/or deposition of amorphous C on their surfaces, which was the typical case for CNT TEM and HRTEM studies.

In summary, for the first time, direct bending force measurements were performed during deformation of multiwalled boron nitride nanotubes by means of a novel AFM−TEM piezodriven holder compatible with a 300 kV JEOL high-resolution field-emission transmission electron microscope. The measured forces ranged between 300 and 900 nN. These, coupled with the observed BNNT dimensions (as measured under a high-resolution imaging mode inside TEM), correspond to bending stresses of ~100−260 MPa and point to elastic BNNT modulus of 0.5−0.6 TPa. Phenomenologically, the present BNNT deformation resembles that of CNTs: under continuous compression, during real-time videorecording in TEM, we observed the momentary formation of consecutive kinks (within a subsecond period of time). However, oppositely to standard CNTs, these kinks did not necessarily appear in the middle tube zones due to pre-existing stress−strain fields within multiple BN walls (these result from a complexity of faceted polygonal multihelix BN shell packing). Up to kink-bending angles of 90°, these defects entirely and momentary disappeared on reloading (within dozens of milliseconds time) in a strict inverse fashion to how they were generated on loading, leaving the tube with the exact same appearance as before the deformation had started. For bending angles exceeding 115°, marginal traces of a residual plastic deformation became visible.

Acknowledgment. We thank B.I. Yakobson for valuable discussions.

Supporting Information Available: Structural (TEM and HRTEM images), chemical (EELS spectrum) and crystallography (electron diffraction pattern) characterization of the initial BNNTs, cross-sectional (the tubes are edge-on) BNNT TEM images taken from a specially prepared cross-sectional TEM sample, results of BNNT elastic modulus estimation (for comparison with the claimed paper data) using an ac mechanical resonance technique,[33,34] and links to real-time movies showing BNNT bending and kinking processes inside TEM using an AFM−TEM holder. This material is available free of charge via the Internet at http://pubs.acs.org.

References

(1) Chopra, N. G.; Luyken, R. I.; Cherrey, K.; Crespi, V. H.; Cohen, M. L.; Loiue, S. G.; Zettl, A. *Science* **1995**, *269*, 966.
(2) Blasé, R.; Rubio, A.; Louie, S. G.; Cohen, M. L. *Europhys. Lett.* **1994**, *28*, 335.
(3) Golberg, D.; Dorozhkin, P. S.; Bando, Y.; Dong, Z. C. *MRS Bull.* **2004**, *29*, 38.
(4) Bai, X. D.; Golberg, D.; Bando, Y.; Zhi, C. Y.; Tang, C.; Mitome, M.; Kurashima, K. *Nano Lett.* **2007**, *7*, 632.
(5) Mele, E. J.; Kral, P. *Phys. Rev. Lett.* **2002**, *88*, 056803.
(6) Zhi, C. Y.; Bando, Y.; Tang, C. C.; Honda, S.; Sato, K.; Kuwahara, H.; Golberg, D. *Angew. Chem., Int. Ed.* **2005**, *44*, 7932.
(7) Wong, E. W.; Sheehan, P. E.; Leiber, C. M. *Science* **1997**, *277*, 1971.
(8) Falvo, M. R.; Clary, G. J.; Taylor, R. M., II; Chi, V.; Brooks, F. P., Jr.; Washburn, S.; Superfine, R. *Nature* **1997**, *389*, 582.
(9) Poncharal, P.; Wang, Z. L.; Ugarte, D.; de Heer, W. A. *Science* **1999**, *283*, 1513.
(10) Salvetat, J.-P.; Briggs, A. D.; Bonard, J.-M., Bacsa, R. R.; Kulik, A. J.; Stockli, T.; Burnham, N. A.; Forro, L. *Phys. Rev. Lett.* **1999**, *82*, 944.
(11) Yu, M. F.; Lourie, O.; Dyer, M. J.; Moloni, K.; Kelly, T. F.; Ruoff, R. S. *Science* **2000**, *287*, 637.
(12) Ding, W.; Calabri, L.; Kohlhaas, K. M.; Chen, X.; Dikin, D. A.; Ruoff, R. S. *Exp. Mech.* **2007**, *47*, 25.
(13) Lu, S. N.; Guo, Z. Y.; Ding, W. Q.; Dikin, D. A.; Lee, J.; Ruoff, R. S. *Rev. Sci. Instrum.* **2006**, *77*, 125101.
(14) Iijima, S.; Brabec, C.; Maiti, A.; Bernholc, J. *J. Chem. Phys.* **1996**, *104*, 2089.
(15) Nakayama, Y.; Akita, S. *New J. Phys.* **2003**, *5*, 128.
(16) Wang, M. S.; Wang, J. Y.; Chen, Q.; Peng, L. M. *Adv. Funct. Mater.* **2005**, *15*, 1825.

(17) Wang, M. S.; Peng, L. M.; Wang, J. Y.; Chen, Q. *Adv. Funct. Mater.* **2006**, *16*, 1462.
(18) Kizuka, T. *Phys. Rev. B* **1999**, *59*, 4646.
(19) Hernandez, E.; Goze, C.; Bernier, P.; Rubio, A. *Phys. Rev. Lett.* **1998**, *80*, 4502.
(20) Yakobson, B. I.; Brabec, C. J.; Bernholc, J. *Phys. Rev. Lett.* **1996**, *76*, 2511.
(21) Kudin, K. N.; Scuseria, G. E.; Yakobson, B. I. *Phys. Rev. B* **2001**, *64*, 235406.
(22) Bettinger, H. F.; Dumitrica, T.; Scuseria, G. E.; Yakobson, B. I. *Phys. Rev. B* **2002**, *65*, 041406.
(23) Dumitrica, T.; Bettinger, H. F.; Scuseria, G. E.; Yakobson, B. I. *Phys. Rev. B* **2003**, *68*, 085412.
(24) Dumitrica, T.; Yakobson, B. I. *Phys. Rev. B* **2005**, *72*, 035418.
(25) Chopra, N. G.; Zettl, A. *Solid State Commun.* **1998**, *105*, 297.
(26) Golberg, D.; Bai, X. D.; Mitome, M.; Tang, C.; Zhi, C. Y.; Bando, Y. *Acta Mater.* **2007**, *55*, 1293.
(27) Tang, C. C.; Bando, Y.; Sato, T.; Kurashima, K. *Chem. Commun.* **2002**, *12*, 1290.
(28) http://www.nanofactory.com.
(29) Landau, L. D.; Lifshits, E. M. *Elasticity Theory*; Pergamon: Oxford, 1986.
(30) Dai, H.; Hafner, J. H.; Rinzler, A. G.; Colbert, D. T.; Smalley, R. E. *Nature* **1996**, *384*, 147.
(31) Celik-Atkas, A.; Zuo, J. M.; Stubbins, J. F.; Tang, C. C.; Bando, Y. *Acta Crystallogr., Sect. A* **2005**, *86*, 133110.
(32) Golberg, D.; Mitome, M.; Bando Y.; Tang, C.; Zhi, C. Y. *Appl. Phys. A* **2007**, http://dx.doi.org/10.1007/s00339-007-3950-8.
(33) Suryavanshi, A. P.; Yu, M.-F.; Wen, J.; Tang, C.; Bando, Y. *Appl. Phys. Lett.* **2004**, *84*, 2527.
(34) Bai, X. D.; Zhi, C. Y.; Tang, C.; Bando, Y.; Golberg, D. unpublished results.
(35) Ding, W. Q.; Calabri, L.; Chen, X. Q.; Kolhaas, K. M.; Ruoff, R. S. *Comp. Sci. Technol.* **2006**, *66*, 1112.
(36) Kis, A.; Csanyi, G.; Salvetat, J.-P.; Lee, T.-N.; Couteau, E.; Kulik, A. J.; Benoit, W.; Brugger, J.; Forro, L. *Nat. Mater.* **2004**, *3*, 153.
(37) Golberg, D.; Bando, Y.; Eremets, M.; Takemura, K.; Kurashima, K.; Tamiya, K.; Yusa, H. *Chem. Phys. Lett.* **1997**, *279*, 191.

NL070863R